Earth and Space Science

RESEARCH ARTICLE
10.1029/2019EA000574

Improved Aerosol Retrievals Over Complex Regions Using NPP Visible Infrared Imaging Radiometer Suite Observations

Yikun Yang[1], Chuanfeng Zhao[1], Lin Sun[2], and Jing Wei[1]

[1]State Key Laboratory of Earth Surface Processes and Resource Ecology, College of Global Change and Earth System Science, Beijing Normal University, Beijing, China, [2]College of Geomatics, Shandong University of Science and Technology, Qingdao, China

Key Points:

- An improved deep blue aerosol retrieval algorithm for VIIRS images is proposed over complex regions
- AOD retrievals agree well with AERONET AOD measurements over the study area
- AOD retrievals are overall better and less biased than VIIRS AOD products

Correspondence to:
C. Zhao, and L. Sun,
czhao@bnu.edu.cn;
sunlin6@126.com

Citation:
Yang, Y., Zhao, C., Sun, L., & Wei, J. (2019). Improved aerosol retrievals over complex regions using NPP Visible Infrared Imaging Radiometer Suite observations. *Earth and Space Science*, *6*, 629–645. https://doi.org/10.1029/2019EA000574

Received 26 JAN 2019
Accepted 8 MAR 2019
Accepted article online 6 APR 2019
Published online 30 APR 2019

Abstract As a new generation of polar-orbiting satellites, NPP VIIRS (National Polar-orbiting Partnership Visible Infrared Imaging Radiometer Suite) provides important supports for the studies of local and global scale climate change, environmental monitoring, and radiant energy balance. This paper proposed an improved deep blue aerosol retrieval algorithm over complex regions based on NPP VIIRS observations. Two improvements were proposed and implemented to the traditional aerosol optical depth (AOD) retrieval algorithm in order to improve the retrieval accuracy, including the construction of the surface reflectance conversion model and aerosol optical parameter acquisition. The retrieval results were extensively evaluated. First, the accuracy of the algorithm was evaluated using AErosol RObotic NETwork ground-based observations, including conditions over different underlying surfaces, different seasons, and different AOD values. Then, the cross validation was carried out between our AOD retrievals and NPP VIIRS aerosol products. The verification results show that our AOD retrievals agree very well with the AErosol RObotic NETwork AOD with coefficient of determination (R^2) ~ 0.85. The improved deep blue algorithm performs well overall under different surface conditions and seasons, while the quality of performance gradually decreases with the increase of AOD. Moreover, the improved algorithm is robust with less bias, root-mean-square error, and relative mean bias in the AOD retrievals and can provide more detailed aerosol information compared with the NPP VIIRS aerosol products. These results suggest that the improved deep blue algorithm can obtain high-precision AOD information, providing better data basis for related researches on air pollution and climate change.

1. Introduction

As an important component of atmosphere, aerosol can change Earth-Atmosphere system radiant energy balance from local to global scales through different processes which include direct effects (Collier & Zhang, 2009; Ghan & Easter, 2006; Quaas et al., 2004; Rap et al., 2013; Yang et al., 2018, 2016; Zhang et al., 2015), indirect effect (Albrecht, 1989; Chylek et al., 2016; Garrett & Zhao, 2006; Liepert & Lohmann, 2001; Lohmann & Feichter, 2005; Rap et al., 2013; Twomey, 1977; Zhao & Garrett, 2015), and semidirect effect (Bauer & Menon, 2012; Johnson, 2005; Koren et al., 2004; Nabat et al., 2015; Randles et al., 2009; Schultze & Rockel, 2018). In particular, aerosol can act as cloud condensation nuclei, which will increase the cloud droplet number concentration and increase cloud albedo (Cruz & Pandis, 1997; Furukawa et al., 2010; Quinn et al., 2017; Spracklen et al., 2011; Twomey, 1977; Zhao et al., 2012; Zhao et al., 2018). By competing for limited water among cloud droplets, increased aerosols could further decrease cloud droplet effective radius (Garrett et al., 2004; Qiu et al., 2017; Wang et al., 2015; Yang et al., 2019; Zhao et al., 2019). Moreover, associated with the increase of cloud condensation nuclei and decrease of cloud droplet effective radius, the lifetime of cloud could also change (Albrecht, 1989; Quinn et al., 2017; Xue et al., 2008).

Aerosols in the atmosphere are from natural and anthropogenic sources (Parsiani & Mèndez, 2008; Skupin et al., 2016), and they vary greatly in space and time (Guo et al., 2017; Kanniah et al., 2014). In arid and semi-arid regions, low vegetation cover over the land makes dust and sand sulfate particles enter the air to form dust aerosol under the action of wind. The fossil fuel burning and other human activities have intensified pollution in urban regions, making urban aerosol research become one focus of the science community and human society (de Almeida Castanho et al., 2008; Jing et al., 2015; Salma et al., 2016; Shi et al., 2018;

Yan et al., 2017). Therefore, a comprehensive understanding of aerosol loadings is essential and critical to climate change, Earth's radiation budget and human health researches (Carmichael et al., 2009; Coakley et al., 1983; Garrett & Zhao, 2006; Ji et al., 2016; Jimenez-Guerrero et al., 2012; Konyukh et al., 1979; Morino et al., 2017; Rind et al., 1992). A key optical parameter of aerosol, aerosol optical depth (AOD), has become an important indicator for measuring aerosol pollution, which is defined as the integrated light extinction over vertical path through the atmosphere.

Satellite remote sensing, as the most direct and effective way to capture the spatial distributions and temporal variations of aerosols over large regions, has been widely used for researches at the local and global scales compared with ground-based Sun photometers (Garcia et al., 2016; Kahn, 2013; Kokhanovsky et al., 2007; Li et al., 2005; Noh et al., 2009; Qin et al., 2016; Sun et al., 2016; Veefkind et al., 1999; Wang, Chen, et al., 2017; Zheng et al., 2017). During past 20 years, a series of sensors have been launched and used in aerosol related researches over land and ocean, such as National Oceanic and Atmospheric Administration Advanced Very High Resolution Radiometer (Geogdzhayev et al., 2004; Hsu et al., 2017), Multi-angle Imaging SpectroRadiometer (Diner et al., 2005; Limbacher & Kahn, 2017), Advanced Along Track Scanning Radiometer (Grey et al., 2006; Guo et al., 2009; Mei et al., 2013; Xue et al., 2009), Polarization and Directionality of the Earth's Reflectance (Deuze et al., 2001), Sea-Viewing Wide Field-Of-View Sensor (Melin et al., 2007; Sayer et al., 2012), Landsat Operational Land Imager (Tian et al., 2018), MODIS (MODerate-Resolution Imaging Spectroradiometer; Levy et al., 2007), VIIRS (Visible Infrared Imaging Radiometer Suite; Jackson et al., 2013; Su et al., 2015; Zhang et al., 2016), and Chinese FengYun Medium Resolution Spectral Imager (Han et al., 2015; Tong et al., 2011). One of the main challenges for the AOD retrieval using satellites is to isolate aerosol particle scattering contributions from satellite recorded signals, which is the superposition of atmospheric path reflectance including atmospheric molecules and aerosol matters as well as surface reflectance signals (Wei et al., 2017). Aerosol optical properties are also key parameters to accurate retrieval of near surface particulate matter, which varies greatly in space and time (Li et al., 2009; Zheng et al., 2017). To meet the increasing demands, a series of satellite aerosol remote sensing retrieval methods and algorithms have been proposed using satellite visible and infrared data.

Based on the spectral radiation measurements from satellite, there are generally four types of AOD retrieval algorithms which include the structure function algorithm (Holben et al., 1992; Sun, 2006; Tanre et al., 1988), the dark target (DT) algorithm (Kaufman, Tanre, et al., 1997), the improved DT algorithm (Levy et al., 2007), and the deep blue (DB) algorithm (Hsu et al., 2004). The structure function algorithm derives the AOD over bright surfaces based on the blurring effect of image, which caused by aerosol particle scattering, with the assumption that the land surface reflectance (LSR) and the intrinsic atmospheric reflectance are invariant for a short time period (Tanre et al., 1988). However, this algorithm does not consider multiple interaction contributions between the land surface and the atmosphere and is greatly affected by weather changes, which will lead to AOD retrieval biases. Over dark land covers such as vegetated areas and dark soils, it has been shown that the LSR at 0.47 and 0.66 μm can be estimated from 2.1 μm with fixed ratios. By comparing the satellite observations and LSR with a preconstructed look-up table (LUT), the DT algorithm can derive the AOD. This DT algorithm was applied to MODIS data and global daily aerosol retrieval products (C4) was published (Kaufman, Tanre, et al., 1997). Recently, the relationships of LSRs at different wavelengths have been further explored and updated to improve the estimation of LSR at visible wavelengths, which is defined as improved DT algorithm here. The improved DT algorithm has been specifically applied to the MODIS, which is also called the second-generation MODIS DT algorithm. Using the International Geosphere/Biosphere Programme's scene map of U.S. Geological Survey surface types, researchers found that the relationships between visible and shortwave infrared (SWIR) channels have a strong dependence on both geometry and surface type. The visible and 2.12-μm surface reflectance relationship is parameterized as a function of both $NDVI_{SWIR}$ and scattering angle (Θ), which has been applied to the new algorithm for MODIS AOD products (C5; Levy et al., 2007). The DT and improved DT aerosol retrieval algorithms can perform well over DT surfaces, but one of the shortcomings is that it cannot retrieve AOD over bright surfaces. In contrast, the DB algorithm extends the aerosol retrieval to the bright surface region and a prior LSR database was used to provide surface reflectance. It was found that the LSR remained low in DB channel over bright regions such as desert and urban areas (Hsu et al., 2004). If the LSR of DB channel can be accurately estimated, then the AOD could be achieved with the expected errors within

$\pm 0.05 \pm 0.2 \times$ AOD over land (Hsu et al., 2013). The DB algorithm was adopted to retrieve global AOD product (C5.1) under the support of static seasonal surface reflectance database, which were precalculated using the Sea-Viewing Wide Field-Of-View Sensor surface reflectance data. An enhanced DB aerosol retrieval algorithm, which considered the impact of vegetation seasonal changes on surface reflectance, was proposed by Hsu et al. (2013). Three schemes were adopted for LSR estimated over natural vegetation areas, urban/built-up and transitional regions, and arid and semiarid surfaces. In addition, aerosol model selection and cloud screening schemes were also improved for producing the MODIS C6 aerosol products.

The VIIRS is a sensor with 22 channels onboard the Suomi National Polar-orbiting Partnership (Suomi NPP) satellite, which can capture visible and infrared signal from 0.4 to 12.4 μm (Hillger et al., 2014). The new generation satellite has higher spatial and temporal resolutions and can be used to retrieve AOD. Previous studies showed that the estimation of surface reflectance and the determination of aerosol model are the main factors affecting the accuracy of AOD retrieval (Tian et al., 2018; Wang et al., 2008). Thus, in this paper, an improved DB algorithm is developed to retrieve high resolution AOD over bright surfaces from VIIRS data. For our improved DB algorithm, two main improvements were implemented: (1) a spectral conversion model between MODIS and VIIRS blue channel was constructed and (2) aerosol optical characteristics over the study area were obtained based on AErosol RObotic NETwork (AERONET) products, which include single scatter albedo (SSA) and asymmetry (g). The AOD retrievals were validated against the AERONET Version 3 Level 2.0 data and compared with the operational VIIRS AOD products VAOOO as well as IVAOT.

The paper is organized as follows. Descriptions of the study area and data are introduced in section 2. Section 3 shows the methodology of the improved DB algorithm. The AOD retrievals are validated in section 4, followed by the discussions and conclusions in sections 5 and 6, respectively.

2. Study Area and Data Sources

2.1. Study Area

In recent years, China is suffering from serious air pollution associated with its rapid growth of economy and population. As the capital of China, Beijing is located in eastern China, which is not only densely populated but also in the heart of the Beijing-Tianjin-Hebei industrial zone, making it a typical area for air pollution research. In addition, the external transport and internal emitted aerosol make the aerosol optical properties of the regions extremely complex. So, in order to examine the adaptability of the improved DB algorithm, Beijing and its surrounding areas (115–118°E, 39–42°N) were selected in this paper. Figure 1 shows the study area along with the AERONET sites, the color of background represents different land cover type (Chen et al., 2014), and the color of the AERONET sites represents elevation information. Totally, five AERONET sites were included, which are Beijing, Beijing_RADI, Beijing-CAMS, XiangHe, and XingLong. Beijing, Beijing_RADI, and Beijing-CAMS are three typical urban sites, which are located in the center of the city. XiangHe and XingLong are located in the suburbs and covered by cultivated land and forests. Except for XingLong, which is situated 899.0 m above sea level, the other four AERONET sites are below 150 m above sea level. Observations at Beijing, Beijing_RADI, Beijing-CAMS, and XiangHe were used to analyze optical characteristics of aerosol particles, and observations at Beijing, Beijing-CAMS, XingLong, and XiangHe were used to evaluate the satellite-based AOD retrievals.

2.2. Data

The data used in this study include the reflectance data at the top of atmosphere (TOA), AOD product and cloud mask from VIIRS, the LSR product from MODIS for the time period from January 2014 to September 2017, and AERONET aerosol products for the time period from January 2012 to September 2017.

2.2.1. NPP VIIRS Data

The VIIRS, the expansion and improvement of Advanced Very High Resolution Radiometer and MODIS sensor, is the second generation imaging radiometer, which boards on the Suomi NPP satellite and crosses equator at 13:30 local time every day. It captures data in 22 sensor data records (Level 1B) from visible to thermal infrared, including 16 moderate-resolution bands (M-bands), 5 high-resolution bands (I-bands), and 1 panchromatic day/night band with the resolutions of 750, 375, and 750 m at nadir, respectively. This satellite is a polar-orbiting satellite with ~3,000-km swath width which allows it to fully sample the Earth every day (Hillger et al., 2014; Yang et al., 2017).

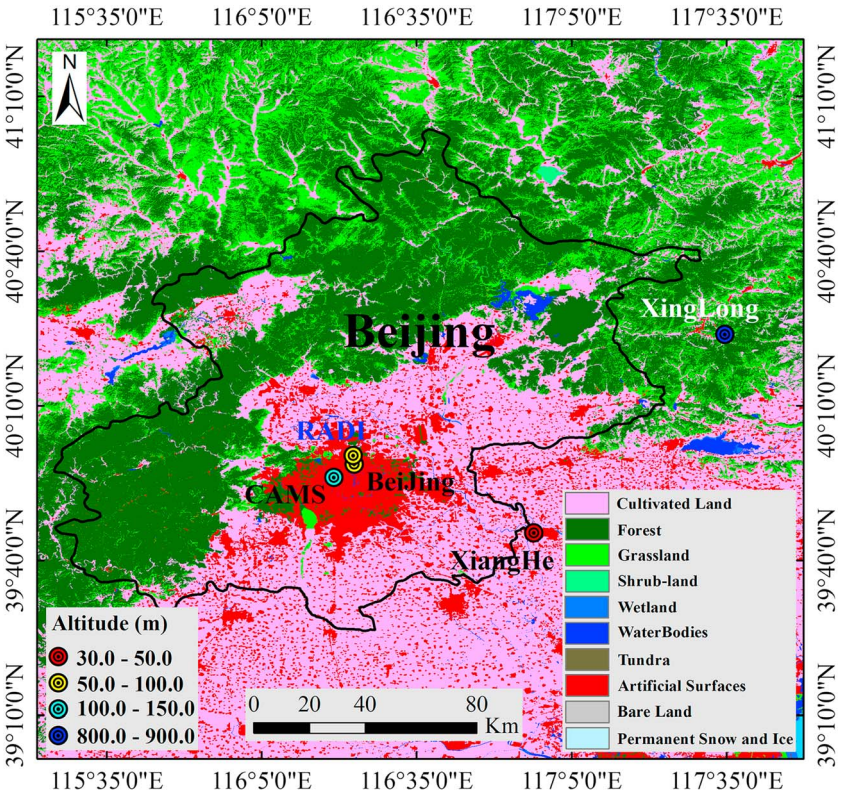

Figure 1. Land cover type and AErosol RObotic NETwork ground-based stations distribution over the study area.

The Level 2 aerosol optical thickness product including Environment Data Records and Intermediate Product (IP) was also used in this study to compare with our aerosol retrievals. The VIIRS AOD IP (IVAOT) only provided AOD at 550 nm with spatial resolution of 750 m. Differently, the VIIRS AOD Environment Data Records (VAOOO) can provide AOD at 10 M-Bands with wavelength range from 412 to 2,250 nm as well as at 550 nm with spatial resolution of 6 km, which is aggregated from the IP measurements (Jackson et al., 2013; Liu et al., 2012). Meanwhile, the mask of inappropriate pixels including cloud/shadow, ice, and snow is also necessary information in aerosol retrieval. Especially, the presence of clouds will lead to cloud contamination, making aerosol retrieval fail. In this study, cloud mask products retrieved using VIIRS cloud mask algorithm were used for unsuitable pixel identification.

2.2.2. Operational MODIS Products

LSR is one of the key factors affecting AOD retrievals. In this study, Aqua Level 2 LSR products (MYD09) were selected to provide high precision surface information, which can reduce the influence of solar zenith angle. The MODIS LSR product consists of seven spectral channels with a spatial resolution of 500 m and an atmospheric correction accuracy of ±(0.005 + 5%) under favorable conditions (not high aerosol amount; Vermote et al., 2015). Table 1 shows the detailed information about the spectral wavelengths and the typical theoretical accuracy of MODIS LSR product (Vermote & Vermeulen, 1999).

Table 1
Detail Information of MODIS LSR Product and Total Theoretical Typical Accuracy

Band	Wavelength (μm)	Center wavelength (μm)	Error
1	0.620–0.670	0.646	0.005
2	0.841–0.876	0.856	0.014
3	0.459–0.479	0.466	0.008
4	0.545–0.565	0.554	0.005
5	1.230–1.250	1.242	0.012
6	1.628–1.652	1.629	0.006
7	2.105–2.155	2.114	0.003

Note. LSR = land surface reflectance; MODIS = MODerate-Resolution Imaging Spectroradiometer.

2.2.3. AERONET Ground-Based Measurements

The AERONET is a ground-based remote sensing aerosol network distributed globally and observed using the CE-318 Sun photometer. It can provide long-term, continuous, and readily accessible database of aerosol optical, microphysical, and radiative properties in diverse aerosol regimes. Specifically, these properties include the observation product of AOD and inversion products of single scattering albedo, asymmetry factor, and phase function. AODs are measured at four wavelengths ranging from 0.34 to 1.02 μm every 15 min with a low uncertainty of 0.01–0.02. Until now, AERONET has released three versions of the data and each

version of the data includes three data quality levels: Level 1.0 (L1.0, unscreened), Level 1.5 (L1.5, cloud-screened and quality controlled), and Level 2.0 (L2.0, quality-assured; Holben et al., 2001). In this study, AERONET Version 3 L2.0 AOD measurements were selected to quantitatively evaluate the reliability of our AOD retrievals. In addition, Version 2 L2.0 inversion products were also used to calculate aerosol optical parameters. Note that Version 3 inversion products were not released during our data processing time, thus it is not used here. Totally, five AERONET sites over the study area were adopted in the analysis. The spatial locations of each AERONET site are also shown in Figure 1. Note that AERONET does not provide the AOD information at 550 nm. Instead, AERONET AOD at 550 nm is calculated based on the Ångström exponent, along with the available AERONET AOD at the two nearest wavelengths (Angstrom, 1964).

3. Methodology

An improved DB aerosol retrieval algorithm was proposed in this study with the a priori LSR database support for VIIRS data over complex land surfaces. The radiant energy acquired by the satellite at the TOA is the result of interaction of electromagnetic waves with the earth's surface and the atmosphere, which can be estimated as follows (Hsu et al., 2004; Tanre et al., 1988),

$$\rho^*(\tau,\theta_s,\varphi_s,\theta_v,\varphi_v)=\rho_0(\tau,\theta_s,\varphi_s,\theta_v,\varphi_v)+T(\theta_s)T(\theta_v)\frac{\rho(\theta_s,\varphi_s,\theta_v,\varphi_v)}{1-\rho(\theta_s,\varphi_s,\theta_v,\varphi_v)S} \quad (1)$$

where τ,θ_s,φ_s,θ_v,and $\varphi_v$are the AOD, solar zenith angle, solar azimuth angle, view zenith angle, and view azimuth angle, respectively; $\rho^*(\tau,\theta_s,\varphi_s,\theta_v,\varphi_v)$ is the TOA reflectance received by the sensor; $\rho_0(\tau,\theta_s,\varphi_s,\theta_v,\varphi_v)$is the atmospheric path reflectance including the joint contribution of the atmospheric molecules and aerosol particles; $\rho(\theta_s,\varphi_s,\theta_v,\varphi_v)$ is the LSR; and T is the total transmittance weakened by the atmospheric molecules and aerosol particles, where$T(\theta_s)$ and $T(\theta_v)$represent the transmittance from the sun to the surface and from the surface to the satellite, respectively; S is the spherical albedo of the atmosphere.

In equation (1), the first term on the right side is the pure atmospheric contribution, and the second term is the combined contribution from the atmosphere and the surface. From equation (1), we can find that as the LSR increases, the TOA reflectance becomes less sensitive to aerosol. As a key parameter of aerosol retrieval, LSR should be accurately estimated. On the other hand, aerosol optical characteristics are other key factors in aerosol retrieval particularly considering that aerosol type has large spatial and temporal variations. Therefore, LSR and aerosol optical characteristics need to be carefully considered in the retrieval of aerosol properties using satellite observations.

3.1. Surface Reflectance Estimation

The LSR has great interannual variations, especially in vegetation and farmland regions during growing seasons. In the traditional aerosol retrieval algorithm, the LSR is usually assumed with little changes over a period of time (Hsu et al., 2013; Sun et al., 2016). Using a minimum synthesis or second minimum synthesis algorithm (Hsu et al., 2004, 2013), the a priori surface reflectance database is often constructed with a time resolution of 1 month. It may lead to large uncertainty to the AOD retrievals, considering the large sensitivity of AOD to surface reflectance as indicated earlier. To solve this problem, two improvements were proposed and implemented for the AOD retrieval in this study. On one hand, an 8-day period MODIS surface reflectance product (MYD09 A1) was used to get more realistic surface reflectance information. Each surface reflectance pixel in the MYD09 A1 product was selected from daily surface reflectance products on the basis of high observation coverage, low satellite zenith angle, the absence of clouds or cloud shadow, and low aerosol loading (Vermote et al., 2015). Compared with the monthly synthesis, 8-day period synthesis has high precision as shown in Table 1 and can reduce the error associated with the surface reflectivity to some extent. On the other hand, due to the difference of spectral response function between the MODIS and VIIRS blue band, a spectral conversion model was constructed in this study using the ASTER measured surface reflectance data.

In the spectral conversion, we approximate the surface as a mixture of vegetation and soil. The vegetation and soils spectral curves were collected from the ASTER spectral library (Baldridge et al., 2009) as endmember spectra, and the mixed pixels were simulated by changing the fraction of vegetation cover (Sun et al.,

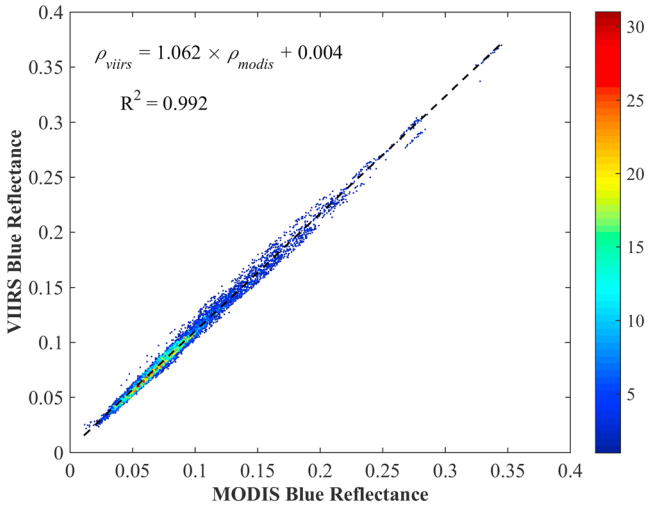

Figure 2. The scatter plot of surface reflectance between MODerate-Resolution Imaging Spectroradiometer (MODIS) and Visible Infrared Imaging Radiometer Suite (VIIRS) blue band. The color represents the density of the scatter, and the dashed line represents the linear regression fitting line.

2010; Tian et al., 2018; Wang et al., 2012). And then the actual surface reflectance can be calculated using the following formula:

$$\rho_i = \frac{\int_{\lambda_1}^{\lambda_2} P(\lambda)S(\lambda)\mathrm{d}\lambda}{\int_{\lambda_1}^{\lambda_2} S(\lambda)\mathrm{d}\lambda} \tag{2}$$

$$\rho = \rho_s \times f_s + \rho_v \times f_v \tag{3}$$

where P is the spectral curve, S represents the spectral response function, ρ_i represents the reflectance in channel i while ρ_s and ρ_v are the MODIS or VIIRS reflectance of soil and vegetation in blue channel which can be obtained from formula (2), f_s and f_v are the proportion of vegetation and soil area, and ρ is the actual surface reflectance of the mixed pixel.

Previous studies have shown that the surface reflectance from two different sensors in close channels can be fitted using a linear regression model, which can reduce the surface reflectance error caused by sensor spectral differences (Sun et al., 2010, 2016). Figure 2 is a scatter plot of the surface reflectance between the MODIS and VIIRS blue channel, in which the color represents the density of the scatter. As seen in Figure 2, the surface reflectance of the MODIS and VIIRS has a strong correlation ($R^2 = 0.99$), and the spectral conversion model is developed as follows:

$$\rho_{\mathrm{viirs}} = 1.062 \times \rho_{\mathrm{modis}} + 0.004 \tag{4}$$

3.2. Assumptions Regarding Aerosol Types

Optical characteristics of aerosol particles are the other important factor affecting the AOD retrieval (Jacobson, 2000; Takemura et al., 2002; Tian et al., 2018). The aerosol characteristics are very complex in Beijing, due to the complicated aerosol sources, including both urban anthropogenic emissions and transport of Beijing-Tianjin-Hebei industrial pollution. In order to obtain more accurate aerosol particle characteristics in this region, and then achieve high precision AOD results, the aerosol SSA and g are statistically analyzed based on observations from AERONET sites from 2012 to 2017. Seasonal variation of aerosol particle characteristics has been investigated. Same as many previous studies (Li et al., 2015; Tian et al., 2018; Wang et al., 2015; Yu et al., 2017), we found that both SSA and g are similar between spring and summer (SS) and similar between autumn and winter (AW). In the 6S (Second Simulation of the Satellite Signal in the Solar Spectrum) radiative transfer model, the atmospheric mode parameters are divided into two types: mid-latitude summer and midlatitude winter. Considering these, SSA and g in both SS and AW have been statistically obtained and implemented into the 6S radiative transfer model. Figure 3 shows the spectral distributions of aerosol SSA and g in both SS and AW over the study area obtained with observations from AERONET sites. As can be seen from the Figure 3, both the SSA and g have large differences between SS and AW. The SSA is significantly higher in SS than in AW, indicating that aerosols in AW have stronger extinction efficiency, which may be related to large fossil fuel combustion in winter heating season. Table 2 further lists the aerosol SSA and g in different seasons used in the AOD retrieval in this study.

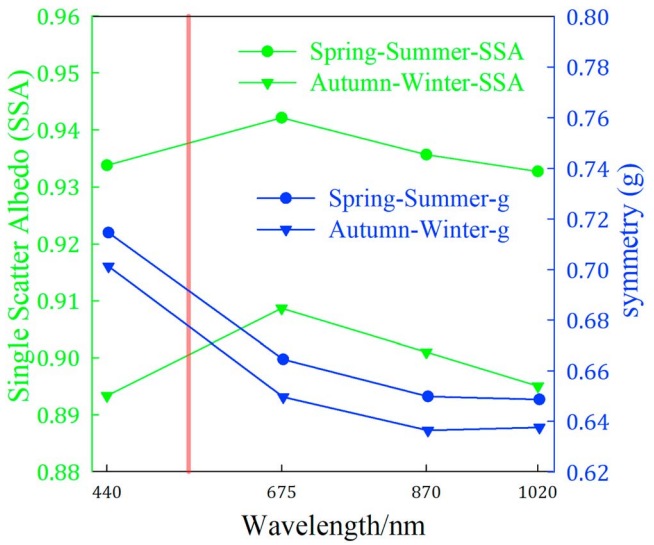

Figure 3. The optical parameters of aerosol over the study area. The green solid line represents the SSA, while the blue solid line is the asymmetry factor, and the dots and triangles represent the SS and AW, respectively; red vertical line indicates wavelength is 550 nm.

3.3. Pixel Selection and AOD Retrieval

The mask identification for unsuitable pixels is also important to the aerosol retrieval. Wrong identification of unsuitable pixels would lead to large errors, even incorrect retrievals of AOD. The VIIRS cloud mask products, which were derived based on a series of reflectance and brightness

Table 2
Optical Properties of Different Aerosol Models Used in AOD Retrieval

Season	Single scattering albedo 0.47/0.55/0.66 μm	Asymmetry parameter 0.47/0.55/0.66 μm
Spring and summer	0.935/0.940/0.942	0.712/0.686/0.666
Autumn and winter	0.895/0.904/0.909	0.698/0.671/0.651

Note. AOD = aerosol optical depth.

temperature threshold tests, were selected for cloud, cloud shadow, and ice/snow screening (Godin & Vicente, 2017).

Similar as the traditional DB retrieval algorithm, the AODs were retrieved using the preconstructed LUT approach. The parameters in LUT are generated based on 6S atmospheric radiative transfer model, which can improve the retrieval efficiency compared to that calculated directly. For clear-sky atmosphere, the 6S model can simulate the solar radiation transmission process in the Earth's atmosphere and calculate the radiance of received by the sensor. In addition, the 6S atmospheric radiative transfer model also effectively considers the absorption of H_2O, CO_2, O_3, and O_2, as well as molecular and aerosol scattering (Kotchenova et al., 2006, 2008; Kotchenova & Vermote, 2007). Then, the parameters in equation (1) are calculated using 6S model for different AOD from 0.0 to 3.0. Finally, The TOA reflectance is calculated for solar and sensor zenith angles from 0° to 60° at intervals of 6°, relative azimuth angles from 0° to 180° in increments of 12° and surface reflectance from 0.01 to 0.15 in increments of 0.01.

Figure 4 shows the flowchart of our improved aerosol retrieval algorithm for VIIRS images. First, we identify unsuitable pixels including cloud, cloud shadow, and ice/snow. Second, based on the assumption of simple

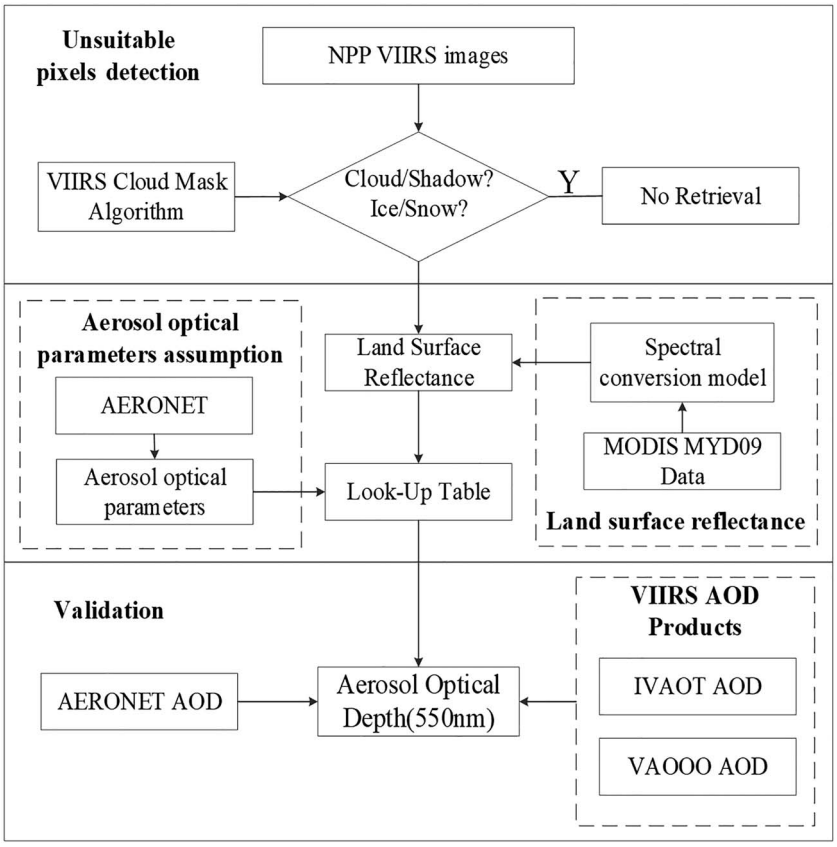

Figure 4. Flowchart of the improved aerosol retrieval algorithm. NPP = National Polar-orbiting Partnership; VIIRS = Visible Infrared Imaging Radiometer Suite; MODIS = MODerate-Resolution Imaging Spectroradiometer; AOD = aerosol optical depth.

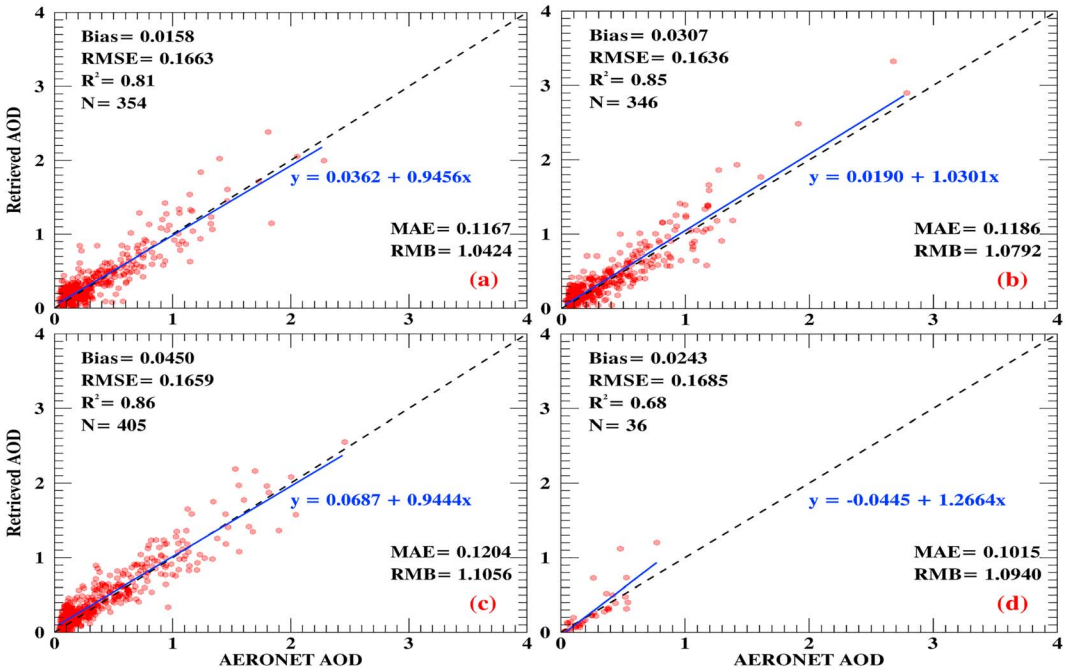

Figure 5. Comparisons of common AODs using improved aerosol retrieval algorithm against AERONET AOD measurements over Beijing (a), Beijing-CAMS (b), XiangHe (c), and XingLong (d). AOD = aerosol optical depth; RMSE = root-mean-square error; MAE = mean absolute error; AERONET = AErosol RObotic NETwork; RMB = relative mean bias.

mixed pixels, the spectral conversion model between MODIS and VIIRS blue channel was constructed, and then the LSR of VIIRS blue channel was calculated. Third, the SSA and g were determined by using the historical AERONET sites observations and a LUT was constructed. Finally, the AODs at 550 nm were retrieved and validated against AERONET data and VIIRS AOD products, respectively.

4. Results and Discussion

This study develops an improved DB aerosol retrieval algorithm based on VIIRS observations, which includes two improvements, the construction of the surface reflectance conversion model and aerosol optical parameter acquisition. The improved retrieval algorithm is then applied to the VIIRS M-Band images over the study areas during 2014–2017. Finally, the VIIRS aerosol products including VAOOO and IVAOT and AERONET Version 3.0 level 2.0 ground-based AOD measurements within the same period were used for validation and comparison. Considering that AERONET only provide AOD values at a single point in space, the AOD retrievals within a sampling window 5 × 5 pixels around the AERONET site were used in the comparison study. At the same time, there are few cases that the retrieved AODs are with large fluctuations and less reliability, which were discarded using the standard deviation. The average of the remaining values is calculated as the retrieved AOD for comparison with the AERONET measurements within the closest moment.

To quantitatively evaluate the precisions of our retrievals, four main evaluation metrics, including the bias (equation (5)), root-mean-square error (RMSE, equation (6)), mean absolute error (MAE, equation (7)), and relative mean bias (RMB, equation (8)) were calculated. Moreover, the linear fitting regression equation is also used to evaluate the performance of our retrieval algorithm, along with the coefficient of determination (R^2). The bias indicates the average deviation between the retrieval result and the measured value. The degree of dispersion of the data can be measured using RMSE. MAE and RMB are also widely used to evaluate the accuracy of two sets of data: MAE can avoid the problem that the errors cancel with each other, thus accurately reflect the actual retrieval error; RMB indicates the average uncertainty estimation of the AOD retrievals, where RMB > 1 and RMB < 1 represents the overestimation and underestimation, respectively.

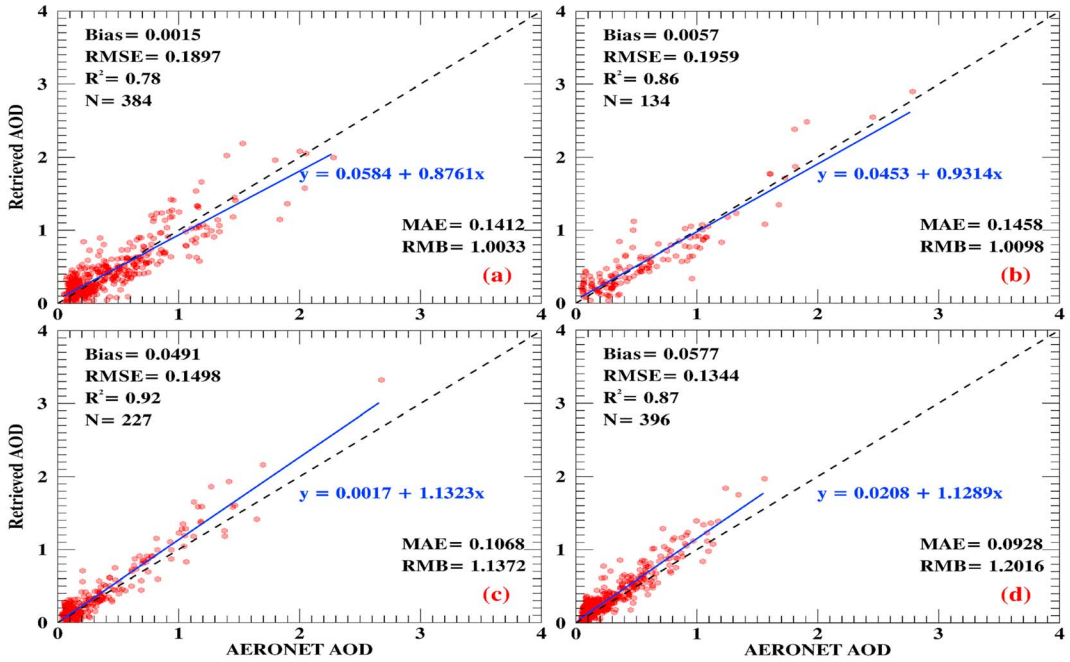

Figure 6. Comparisons of AODs from the improved aerosol retrieval algorithm against AERONET AOD measurements in different seasons: (a) spring, (b) summer, (c) autumn, and (d) winter. AOD = aerosol optical depth; RMSE = root-mean-square error; MAE = mean absolute error; AERONET = AErosol RObotic NETwork; RMB = relative mean bias.

$$\mathrm{Bias} = \frac{1}{n}\sum_{i=0}^{n}\left(\mathrm{AOD}^{i}_{\mathrm{Retrieval}} - \mathrm{AOD}^{i}_{\mathrm{AERONET}}\right) \tag{5}$$

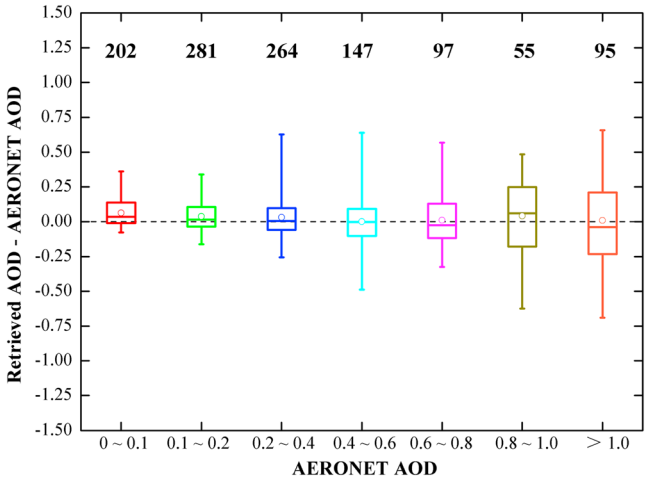

Figure 7. Box plots of AOD differences (AOD retrievals-AERONET AODs) versus AERONET AOD. For each box whisker, the low and upper solid lines in the box demonstrate the 25th and 75th percentiles of the AOD biases, the lower and upper whiskers are the minimum and maximum of the AOD error, the middle line in each box represents the median value of the AOD biases, the middle circle in each box shows the mean value of the AOD retrieval biases, the dashed line is $y = 0$, and the number above each box refers to the corresponding samples in each bin of AERONET AODs. AOD = aerosol optical depth; AERONET = AErosol RObotic NETwork.

$$\mathrm{RMSE} = \sqrt{\frac{1}{n}\sum_{i=0}^{n}\left(\mathrm{AOD}^{i}_{\mathrm{Retrieval}} - \mathrm{AOD}^{i}_{\mathrm{AERONET}}\right)^{2}} \tag{6}$$

$$\mathrm{MAE} = \frac{1}{n}\sum_{i=0}^{n}\left|\mathrm{AOD}^{i}_{\mathrm{Retrieval}} - \mathrm{AOD}^{i}_{\mathrm{AERONET}}\right| \tag{7}$$

$$\mathrm{RMB} = \overline{\mathrm{AOD}_{\mathrm{Retrieval}}}\,/\,\overline{\mathrm{AOD}_{\mathrm{AERONET}}} \tag{8}$$

4.1. Validation With AERONET AOD Measurements

Same as Huang et al. (2016), the performance of retrieval algorithm is evaluated by comparing with the AERONET AOD measurements. Huang et al. (2016) found that the VIIRS AOD exhibits an overall global bias against AERONET of −0.0008 with RMSE as 0.12. They also suggested that the retrieval errors are linked to specific regions, seasons, surface characteristics, and aerosol types. We here investigate the performance of our retrieval algorithm over heavy polluted region around Beijing for the study period.

4.1.1. Site and Regional Performance

The Version 3.0 AERONET aerosol product at four sites including Beijing, Beijing-CAMS, XiangHe, and XingLong over the study area are used to verify the AOD retrievals from January 2014 to September 2017. Figure 5 shows the comparison results of retrieved AOD against the AERONET AOD, in which the dotted line represents the 1:1 line and the solid blue line represents the linear fitting regression line. More

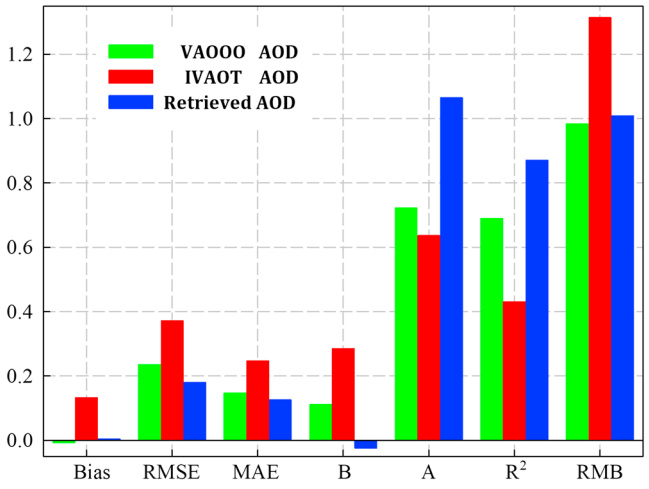

Figure 8. The verification results for the two Visible Infrared Imaging Radiometer Suite aerosol products (VAOOO and IVAOT) and our AOD retrievals using AERONET ground AOD. The green, red, and blue represents VAOOO, IVAOT, and the AOD retrievals using the improved deep blue algorithm, respectively. The seven indicators used here are Bias, RMSE, MAE, R^2, MAB, A, and B, where A and B represent the slope and intercept of the regression line. AOD = aerosol optical depth; RMSE = root-mean-square error; MAE = mean absolute error; RMB = relative mean bias.

than 340 samples have been used for each site of Beijing, Beijing-CAMS, and XiangHe. In contrast, there are only 36 samples at XingLong site, since the site has no longer provided observation data since November, 2014. Figure 5 shows that the AOD is mainly between 0 and 1.0. Based on the four evaluation metrics we introduced, the aerosol retrievals are highly consistent with the AERONET ground-based observations. The linear regression line is basically the same as the 1:1 line. Simultaneously, the coefficient of determination (R^2) is large, the bias is less than 0.05, and the RMSE (0.16–0.17) and the MAE (0.10–0.12) are small overall. Note that the RMSE errors are slightly larger for our retrievals over the study region compared to that found for the VIIRS NPP AOD product over the global land by Huang et al. (2016), which is 0.12. Compared with XiangHe and XingLong, Beijing and Beijing-CAMS are two typical urban sites, with the surface reflectance less subject to seasonal changes in vegetation. Correspondingly, the AOD retrievals show a high precision with an average overestimation of 4.24% (RMB = 1.0424) and 7.92% (RMB = 1.0792) at Beijing and Beijing-CAMS, respectively. Differently, the underlying surface of the XiangHe and XingLong sites is mainly vegetation associated with which there are relatively large aerosol retrieval errors, overestimations of 10.56% and 9.4%, respectively.

4.1.2. Seasonal Performance

Both aerosol type and surface reflectance have significant seasonal variations. Thus, further research is carried out to investigate the efficiency and stability of the improved aerosol retrieval algorithm in different seasons, which is shown in Figure 6. There are totally 384, 134, 227, and 396 pairs of samples in spring, summer, autumn, and winter, respectively. For different seasons, the AOD retrievals agree well with the AERONET AODs with coefficient of determination (R^2) between 0.78 and 0.92. However, Figure 6 shows that there are obvious seasonal differences in the performance of our improved retrieval algorithm. Compared with AW, the retrieved AODs have lower biases with average values of 0.0015 and 0.0057 and lower RMBs of 1.0033 and 1.0098 in SS. However, the retrieved AODs have larger correlations and lower RMSE with AERONET AODs in AW than in SS. For example, the improved AOD retrievals agree well with AERONET AODs (R^2 = 0.92 and 0.87), with the average RMSEs of 0.1491 and 0.1344 and MAEs of 0.1068 and 0.0928 in AW, respectively. Different from the other three seasons, the aerosol retrievals have relatively large errors in winter. This is likely due to the errors in aerosol particle characteristics such as SSA and g, because the coal burning over the study area in winter makes the regional aerosol optical characteristics more complicated.

4.1.3. Variation of Retrieval Biases With AOD

Figure 7 shows the boxplots of AOD retrieval biases (AOD retrievals-AERONET AODs) against the ground-based AOD observations over the study region from 2014 to 2017. For each box whisker, the low and upper solid lines in the box demonstrate the 25th and 75th percentiles of the AOD biases, the lower and upper whiskers are the minimum and maximum of the AOD error, the middle line in each box represents the median value of the AOD biases, the middle circle in each box shows the mean value of the AOD retrieval biases, the dashed line is $y = 0$, and the number above each box refers to the corresponding samples in each bin of AERONET AODs. Overall, as mention earlier, the AOD retrievals are mainly between 0 and 1.0, which account for 91.67% of the total samples. The mean AOD retrieval bias is 0.09 with upper and lower quantile values of 0.04 and −0.01, respectively, when AOD is between 0.0 and 0.1. When AOD increases, the mean AOD retrieval bias along with the upper and lower quantiles increases. For example, when AOD is between 0.8 and 1.0, the mean AOD retrieval bias is 0.25 with upper and lower quantile values of 0.25 and −0.18, respectively, which are larger than that when AOD is between 0.0 and 0.1.

4.2. Comparison With Operational AOD Products

VIIRS AOD products have been fully evaluated by previous studies (Huang et al., 2016; Liu et al., 2012). Particularly, Huang et al. (2016) showed good performance of VIIRS AOD products compared to AERONET measurements and investigated various influential factors to the uncertainties of VIIRS AOD. In this study, VIIRS aerosol products are also used for cross validation of our retrieval algorithms over the

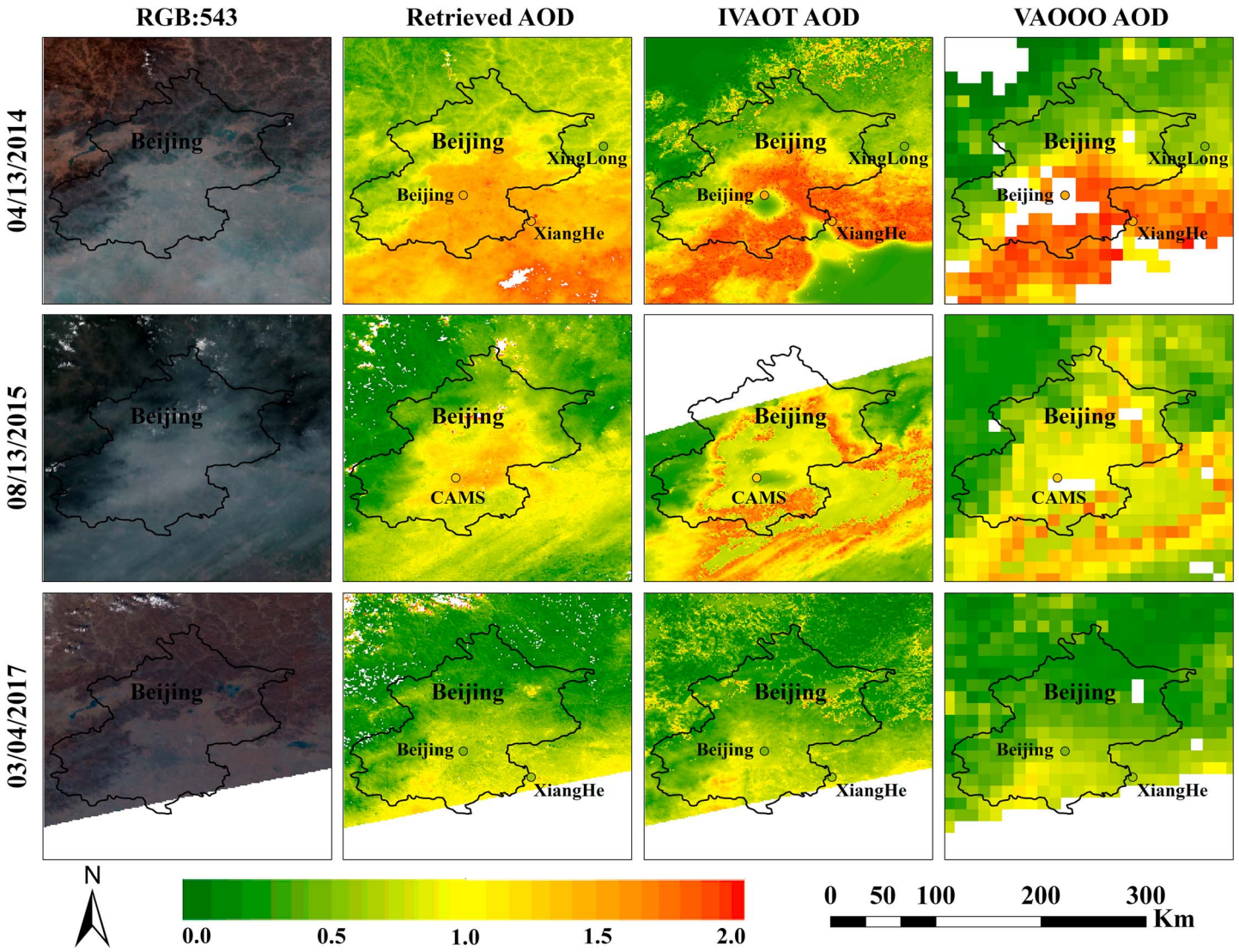

Figure 9. Comparisons of spatial distributions of retrieved AOD (the second column) with IVAOT AOD (the third column) and VAOOO AOD (the fourth column) over the study area, along with the original satellite true color composite images (the first column), for observation time of 13 April 2014 (the first row), 13 August 2015 (the second row), and 4 March 2017 (the third row). AOD = aerosol optical depth.

study region from 2014 to 2017, which include IVAOT and VAOOO with resolution of 750 m and 6 km at nadir, respectively. Figure 8 shows the verification results for the two VIIRS aerosol products and our AOD retrievals using AERONET ground-based aerosol data. Same as what we did earlier, seven indicators are calculated including Bias, RMSE, MAE, R^2, MAB, A, and B, where A and B represent the slope and intercept of the linear fitting regression line. VAOOO AOD and our AOD retrievals have a small negative bias, while IVAOT AOD has a larger positive bias. Both VAOOO and IVAOT AODs have large RMSE and low coefficient of determination (~0.6) compared with AERONET AOD. In addition, the VAOOO AOD has higher accuracy than IVAOT AOD, which overestimate (RMB = 1.31) aerosols results seriously. Our AOD retrievals are more accurate with Bias = 0.01, R^2 = 0.87, and MAE = 0.12. Moreover, the RMSE for our retrievals is about 52% smaller than that for IVAOT. Meanwhile, VAOOO AOD and our AOD retrievals have the similar RMB but VAOOO AOD has a larger intercept (B = 0.11), which indicates that VAOOO overestimates AOD when AOD is small. The verification results indicate that our aerosol retrieval algorithm is robust and can retrieve AOD with more accuracy than the VIIRS aerosol products.

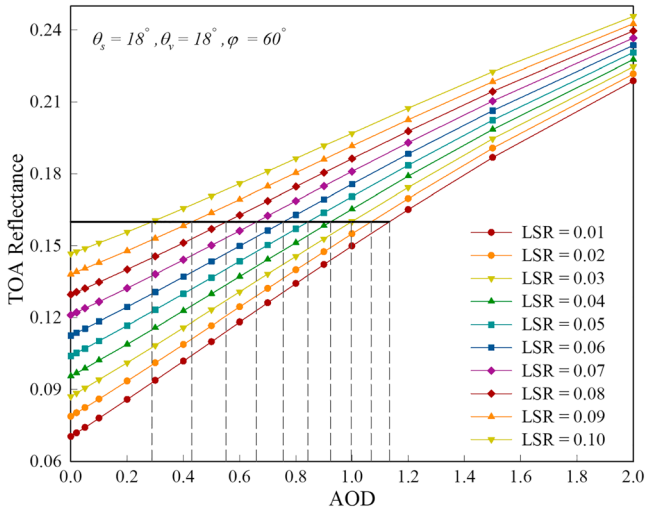

Figure 10. Influence of LSR error on AOD retrieval with changes of TOA reflectance. The results are from the 6S radiative transfer model simulations. LSR = land surface reflectance; AOD = aerosol optical depth; TOA = top of atmosphere.

4.3. Spatial Distributions of AOD

Three cases were selected to display the spatial distribution of AOD from our retrievals and VIIRS products on 13 April 2014, 13 August 2015, and 4 March 2017, as shown in Figure 9. The four columns from left to right represent true color composite images (RGB:543), retrieved AOD, IVAOT AOD, and VAOOO AOD, respectively. The blank areas represent those with invalid aerosol retrievals. The color of AERONET sites shows the AOD value from the AERONET measurements, which has the same color definition as retrieved AOD. The VIIRS aerosol algorithm did not retrieve aerosols over inappropriate situations (cloud, bright surfaces, etc.), for which the AOD in the IVAOT aerosol product was obtained using an interpolation method based on the retrieved aerosol results and operational aerosol chemical transport model results. Even though the IVAOT AOD products can provide aerosol for every pixel, the results have a large bias over bright urban surface, as well as over vegetation and water areas. The VAOOO aerosol product did not adopt the interpolation method for those inappropriate conditions. As shown in Figure 9, the VAOOO AOD products have a large number of missing values with relatively poor spatial continuity. Compared with the two VIIRS operational aerosol products, our retrieved AODs are more consistent with the AERONET AOD measurements with smaller biases. Actually, our retrieved AODs show more consistent spatial distribution with the true color composite images than the two VIIRS operational aerosol products of AOD.

5. Discussions

Surface reflectance and aerosol particle characteristics are key factors affecting aerosol retrieval (Chu et al., 2003). The 8-day synthetic surface reflectance database can reduce the surface reflectance error caused by the surface changes to a certain extent and then reduce the errors in the aerosol retrieval. More accurate aerosol particle characteristics could also be obtained based on the AERONET sites observations, which can be further used in the satellite-based aerosol retrieval. However, our retrievals could still have certain uncertainties due to the spatiotemporal variations of the surface type and aerosol particle characteristics. We here briefly investigate the effects of LSR error and aerosol optical parameter error on aerosol retrievals based on the 6S atmospheric radiative transfer model simulation.

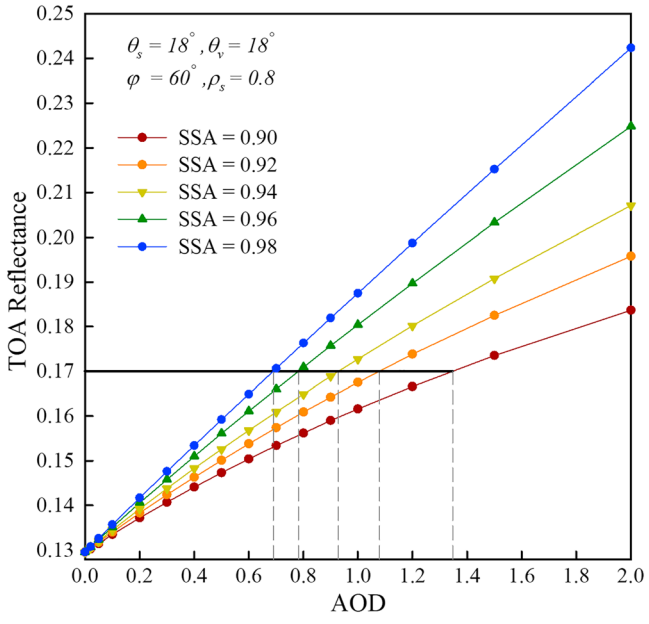

Figure 11. The variation of simulated TOA reflectance with the SSA and AOD by the 6S radiative transfer model. AOD = aerosol optical depth; LSR = land surface reflectance; TOA = top of atmosphere.

5.1. LSR

In this paper, the influence of LSR on aerosol retrievals was simulated using the 6S radiative transfer model with 18°, 18°, and 60° for the satellite zenith angle, solar zenith angle, and relative azimuth angle under LSR between 0.01 and 0.1 with the step of 0.01. Previous studies showed that the LSR of most surface cover types are less than 0.1 (Wei & Sun, 2017). Figure 10 shows the simulation results. The black horizontal line represents the TOA reflectance of 0.16. It indicates that LSR have a significant impact on aerosol retrievals. As LSR increases, the sensitivity of AOD retrieval to surface reflection also increases. Quantitatively, when AOD is equal to 1.0 with TOA reflectance of 0.16, the surface reflectance error of 0.01 can cause an AOD retrieval error of approximately 0.08 (LSR ~ 0.04), while the error of AOD retrieval would reach to approximately 0.15 (LSR ~ 0.09), similar to previous simulation results (Kaufman, Wald, et al., 1997; Tian et al., 2018; Wang, Sun, et al., 2017). Therefore, it is critical to estimate the LSR especially in urban areas. Figure 10 also shows that the sensitivity of AOD retrieval to surface

reflectance is dependent on the TOA reflectance. When TOA reflectance increases, that is, the contributions of aerosol to the radiant energy at the TOA increase, but the sensitivity of AOD retrievals to surface reflectance decreases. The sensitivity of aerosol to change of TOA reflectance is high with large slopes approximately 0.08 over the dark regions and 0.05 over bright regions. Previous studies (e.g., Wei et al., 2018) showed similar findings while the values are slightly different due to the wavelength differences for the MODIS simulation. Overall, the LSR error can to some extent cause error of AOD retrieval.

5.2. Aerosol Optical Parameters

The effect of aerosol SSA on the satellite-based AOD retrieval is also investigated with the 6S radiative transfer model simulations with the same parameters as shown in section 5.1 except that the LSR was set to 0.08 and the SSA was set from 0.90 to 0.98 in an increment of 0.02. Figure 11 demonstrates the variation of simulated TOA reflectance with the SSA and AOD. Different from the surface reflectance, the sensitivity of AOD retrievals to SSA increases with the decreasing SSA for a fixed TOA reflectance, which is basically consistent with that found in previous studies (e.g., Hsu et al., 2004). Meanwhile, the sensitivity also increases with the increasing TOA reflectance. Compared with the study of Tian et al. (2018), SSA has a greater impact on AOD retrieval in high surface reflectance regions. On the other hand, the impact of SSA on AOD retrievals increases with AOD. Thus, there is no doubt that SSA is crucial for the AOD retrieval.

6. Conclusions

In this paper, an improved DB aerosol retrieval algorithm was proposed based on VIIRS data. Two main improvements were implemented in the new retrieval algorithm including the estimation of LSR and the statistics of aerosol particle optical characteristics. In order to reduce the influence caused by the difference in LSR, the spectral conversion model between MODIS and VIIRS blue channel was constructed using the measured spectral data under the assumption of simple mixed pixels. In addition, based on the historical aerosol optical properties from AERONET site observations, the aerosol SSA and asymmetry factor were determined and a more accurate aerosol retrieval LUT was constructed using the 6S atmospheric radiative transfer model. Then, the improved retrieval algorithm was applied to the VIIRS data with the resolutions of 750 m at nadir from January 2014 to September 2017.

To test and validate the performances of the improved aerosol retrieval algorithm, ground-based AERONET AOD data with version 3, VIIRS aerosol products including IVOOO and IVAOT with the resolutions of 6 and 0.75 km were used for comparison. Seven statistical indicators are introduced for the evaluation of retrieval algorithm performance, which include Bias, RMSE, MAE, R^2, MAB, A, and B, where A and B represent the slope and intercept of the regression line.

The results show that the improved aerosol retrieval algorithm performs well compared to the AERONET AOD, with high coefficient of determination (R^2) of 0.81, 0.85, 0.86, and 0.68 at Beijing, Beijing-CAMS, XiangHe, and XingLong, respectively. Our improved aerosol retrieval algorithm also shows much better performance than the VIIRS aerosol products based on seven statistical indicators we introduced, compared with the AERONET AOD. The above results indicate that the proposed improved aerosol retrieval algorithm can obtain more accurate AOD results compared to current VIIRS AOD products.

Acknowledgments
This work was supported by the National Natural Science Foundation of China (grants 91837204 and 41575143), the National Key R&D Program on Monitoring, Early Warning and Prevention of Major Natural Disasters (grant 2017YFC1501403), the State Key Laboratory of Earth Surface Processes and Resource Ecology (2017-ZY-02), and the Fundamental Research Funds for the Central Universities (2017EYT18 and 312231103). The VIIRS products are available from the Atmospheric Administration (NOAA)'s Comprehensive Large Array-data Stewardship System (CLASS) website (https://www.bou.class.noaa.gov/). AERONET measurements are available from the NASA Godard Space Flight Center (https://aeronet.gsfc.nasa.gov/). The MODIS data are available from Atmosphere Archive & Distribution System (LAADS) Distributed Active Archive (https://ladsweb.modaps.eosdis.nasa.gov/). The land cover type data are download from GLOBELAND30 (http://www.globallandcover.com/GLC30Download/), and the ASTER measured surface reflectance data are collected from ASTER spectral library (https://speclib.jpl.nasa.gov/).

References

Albrecht, B. A. (1989). Aerosols, cloud microphysics, and fractional cloudiness. *Science*, *245*(4923), 1227–1230. https://doi.org/10.1126/science.245.4923.1227

Angstrom, A. (1964). The parameters of atmospheric turbidity. *Tellus*, *16*(1), 64–75. https://doi.org/10.1111/j.2153-3490.1964.tb00144.x

Baldridge, A. M., Hook, S. J., Grove, C. I., & Rivera, G. (2009). The ASTER spectral library version 2.0. *Remote Sensing of Environment*, *113*(4), 711–715. https://doi.org/10.1016/j.rse.2008.11.007

Bauer, S. E., & Menon, S. (2012). Aerosol direct, indirect, semidirect, and surface albedo effects from sector contributions based on the IPCC AR5 emissions for preindustrial and present-day conditions. *Journal of Geophysical Research*, *117*, D01206. https://doi.org/10.1029/2011JD016816

Carmichael, G. R., Adhikary, B., Kulkarni, S., D'Allura, A., Tang, Y., Streets, D., et al. (2009). Asian aerosols: Current and year 2030 distributions and implications to human health and regional climate change. *Environmental Science & Technology*, *43*(15), 5811–5817. https://doi.org/10.1021/es8036803

Chen, J., Ban, Y., & Li, S. (2014). Open access to Earth land-cover map. *Nature*, *514*(7523), 434–434. https://doi.org/10.1038/514434c

Chu, D. A., Kaufman, Y. J., Zibordi, G., Chern, J. D., Mao, J., Li, C. C., & Holben, B. N. (2003). Global monitoring of air pollution over land from the Earth Observing System-Terra Moderate Resolution Imaging Spectroradiometer (MODIS). *Journal of Geophysical Research*, *108*(D21), 4661. https://doi.org/10.1029/2002JD003179

Chylek, P., Vogelsang, T. J., Klett, J. D., Hengartner, N., Higdon, D., Lesins, G., & Dubey, M. K. (2016). Indirect aerosol effect increases CMIP5 models' projected Arctic warming. *Journal of Climate*, *29*(4), 1417–1428. https://doi.org/10.1175/jcli-d-15-0362.1

Coakley, J. A., Cess, R. D., & Yurevich, F. B. (1983). The effect of tropospheric aerosols on the earths radiation budget—A parameterization for climate models. *Journal of the Atmospheric Sciences*, *40*(1), 116–138. https://doi.org/10.1175/1520-0469(1983)040<0116:Teotao>2.0.Co;2

Collier, J. C., & Zhang, G. J. (2009). Aerosol direct forcing of the summer Indian monsoon as simulated by the NCAR CAM3. *Climate Dynamics*, *32*(2–3), 313–332. https://doi.org/10.1007/s00382-008-0464-9

Cruz, C. N., & Pandis, S. N. (1997). A study of the ability of pure secondary organic aerosol to act as cloud condensation nuclei. *Atmospheric Environment*, *31*(15), 2205–2214. https://doi.org/10.1016/s1352-2310(97)00054-x

de Almeida Castanho, A. D., Martins, J. V., & Artaxo, P. (2008). MODIS aerosol optical depth retrievals with high spatial resolution over an urban area using the critical reflectance. *Journal of Geophysical Research*, *113*, D02201. https://doi.org/10.1029/2007JD008751

Deuze, J. L., Bréon, F. M., Devaux, C., Goloub, P. H., Herman, M., Lafrance, B., et al. (2001). Remote sensing of aerosols over land surfaces from POLDER-ADEOS-1 polarized measurements. *Journal of Geophysical Research*, *106*(D5), 4913–4926. https://doi.org/10.1029/2000JD900364

Diner, D. J., Martonchik, J. V., Kahn, R. A., Pinty, B., Gobron, N., Nelson, D. L., & Holben, B. N. (2005). Using angular and spectral shape similarity constraints to improve MISR aerosol and surface retrievals over land. *Remote Sensing of Environment*, *94*(2), 155–171. https://doi.org/10.1016/j.res.2004.09.009

Furukawa, T., Takahashi, Y. J. A. C., & Discussions, P. (2010). Metal complexation inhibits the effect of oxalic acid in aerosols as cloud condensation nuclei (CCN). *Atmospheric Chemistry & Physics Discussions*, *10*(11), 27,099–27,134. https://doi.org/10.5194/acpd-10-27099-2010

Garcia, R. D., Garcia, O. E., Cuevas, E., Cachorro, V. E., Barreto, A., Guirado-Fuentes, C., et al. (2016). Aerosol optical depth retrievals at the Izana atmospheric observatory from 1941 to 2013 by using artificial neural networks. *Atmospheric Measurement Techniques*, *9*(1), 53–62. https://doi.org/10.5194/amt-9-53-2016

Garrett, T. J., Zhao, C., Dong, X., Mace, G. G., & Hobbs, P. V. (2004). Effects of varying aerosol regimes on low-level Arctic stratus. *Geophysical Research Letters*, *31*, L17105. https://doi.org/10.1029/2004GL019928

Garrett, T. J., & Zhao, C. F. (2006). Increased Arctic cloud longwave emissivity associated with pollution from mid-latitudes. *Nature*, *440*(7085), 787–789. https://doi.org/10.1038/nature04636

Geogdzhayev, I. V., Mishchenko, M. I., Liu, L., & Remer, L. (2004). Global two-channel AVHRR aerosol climatology: Effects of stratospheric aerosols and preliminary comparisons with MODIS and MISR retrievals. *Journal of Quantitative Spectroscopy & Radiative Transfer*, *88*(1–3), 47–59. https://doi.org/10.1016/j.jqsrt.2004.03.024

Ghan, S. J., & Easter, R. C. (2006). Impact of cloud-borne aerosol representation on aerosol direct and indirect effects. *Atmospheric Chemistry and Physics*, *6*(12), 4163–4174. https://doi.org/10.5194/acp-6-4163-2006

Godin, R., and G. Vicente (2017), Joint Polar Satellite System (JPSS) Operational Algorithm Description (OAD) Document for VIIRS Cloud Mask (VCM) Environmental Data Records (EDR) Software JPSS Electronic Signature Page.

Grey, W. M. F., North, P. R. J., Los, S. O., & Mitchell, R. M. (2006). Aerosol optical depth and land surface reflectance from multiangle AATSR measurements: Global validation and intersensor comparisons. *IEEE Transactions on Geoscience and Remote Sensing*, *44*(8), 2184–2197. https://doi.org/10.1109/tgrs.2006.872079

Guo, J., Xia, F., Zhang, Y., Liu, H., Li, J., Lou, M., et al. (2017). Impact of diurnal variability and meteorological factors on the PM2.5 - AOD relationship: Implications for PM2.5 remote sensing. *Environmental Pollution*, *221*, 94–104. https://doi.org/10.1016/j.envpol.2016.11.043

Guo, J., Xue, Y., Cao, C., Zhang, H., Guang, J., Zhang, X., & Li, X. (2009). A synergic algorithm for retrieval of aerosol optical depth over land. *Advances in Atmospheric Sciences*, *26*(5), 973–983. https://doi.org/10.1007/s00376-009-7218-4

Han, W., L. Tong, and Y. Chen (2015), Aerosol retrieval over urban area by syngertic use of Feng Yun-3C MERSI and Terra MODIS data, IEEE International Conference on Smart City/socialcom/sustaincom, 108-111, doi:https://doi.org/10.1109/SmartCity.2015.55.

Hillger, D., Seaman, C., Liang, C., Miller, S., Lindsey, D., & Kopp, T. (2014). Suomi NPP VIIRS imagery evaluation. *Journal of Geophysical Research: Atmospheres*, *119*, 6440–6455. https://doi.org/10.1002/2013JD021170

Holben, B., Vermote, E., Kaufman, Y. J., Tanre, D., & Kalb, V. (1992). Aerosol retrieval OVER land from AVHRR data - application for atmospheric correction. *IEEE Transactions on Geoscience and Remote Sensing*, *30*(2), 212–222. https://doi.org/10.1109/36.134072

Holben, B. N., Tanré, D., Smirnov, A., Eck, T. F., Slutsker, I., Abuhassan, N., et al. (2001). An emerging ground-based aerosol climatology: Aerosol optical depth from AERONET. *Journal of Geophysical Research*, *106*(D11), 12,067–12,097. https://doi.org/10.1029/2001JD900014

Hsu, N. C., Jeong, M. J., Bettenhausen, C., Sayer, A. M., Hansell, R., Seftor, C. S., et al. (2013). Enhanced Deep Blue aerosol retrieval algorithm: The second generation. *Journal of Geophysical Research: Atmospheres*, *118*, 9296–9315. https://doi.org/10.1002/jgrd.50712

Hsu, N. C., Lee, J., Sayer, A. M., Carletta, N., Chen, S. H., Tucker, C. J., et al. (2017). Retrieving near-global aerosol loading over land and ocean from AVHRR. *Journal of Geophysical Research: Atmospheres*, *122*, 9968–9989. https://doi.org/10.1002/2017JD026932

Hsu, N. C., Tsay, S. C., King, M. D., & Herman, J. R. (2004). Aerosol properties over bright-reflecting source regions. *IEEE Transactions on Geoscience and Remote Sensing*, *42*(3), 557–569. https://doi.org/10.1109/tgrs.2004.824067

Huang, J., Kondragunta, S., Laszlo, I., Liu, H., Remer, L. A., Zhang, H., et al. (2016). Validation and expected error estimation of Suomi-NPP VIIRS aerosol optical thickness and Angstrom exponent with AERONET. *Journal of Geophysical Research: Atmospheres*, *121*, 7139–7160. https://doi.org/10.1002/2016JD024834

Jackson, J. M., Liu, H., Laszlo, I., Kondragunta, S., Remer, L. A., Huang, J., & Huang, H.-C. (2013). Suomi-NPP VIIRS aerosol algorithms and data products. *Journal of Geophysical Research: Atmospheres*, *118*, 12,673–12,689. https://doi.org/10.1002/2013jd020449

Jacobson, M. Z. (2000). A physically-based treatment of elemental carbon optics: Implications for global direct forcing of aerosols. *Geophysical Research Letters*, *27*(2), 217–220. https://doi.org/10.1029/1999gl010968

Ji, Z., Wang, G., Pal, J. S., & Yu, M. (2016). Potential climate effect of mineral aerosols over West Africa. Part I: model validation and contemporary climate evaluation. *Climate Dynamics*, *46*(3–4), 1223–1239. https://doi.org/10.1007/s00382-015-2641-y

Jimenez-Guerrero, P., Pedro Montavez, J., Jose Gomez-Navarro, J., Jerez, S., & Lorente-Plazas, R. (2012). Impacts of climate change on ground level gas-phase pollutants and aerosols in the Iberian Peninsula for the late XXI century. *Atmospheric Environment*, *55*, 483–495. https://doi.org/10.1016/j.atmosenv.2012.02.048

Jing, J., Wu, Y., Tao, J., Che, H., Xia, X., Zhang, X., et al. (2015). Observation and analysis of near-surface atmospheric aerosol optical properties in urban Beijing. *Particuology*, *18*, 144–154. https://doi.org/10.1016/j.partic.2014.03.013

Johnson, B. T. (2005). The semidirect aerosol effect: Comparison of a single-column model with large eddy simulation for marine stratocumulus. *Journal of Climate*, *18*(1), 119–130. https://doi.org/10.1175/jcli-3233.1

Kahn, R. A. (2013), Satellite remote sensing: Aerosol measurements.
Kanniah, K. D., Lim, H. Q., Kaskaoutis, D. G., & Cracknell, A. P. (2014). Investigating aerosol properties in peninsular Malaysia via the synergy of satellite remote sensing and ground-based measurements. *Atmospheric Research*, *138*, 223–239. https://doi.org/10.1016/j.atmosres.2013.11.018
Kaufman, Y. J., Tanre, D., Remer, L. A., Vermote, E. F., Chu, A., & Holben, B. N. (1997). Operational remote sensing of tropospheric aerosol over land from EOS moderate resolution imaging spectroradiometer. *Journal of Geophysical Research*, *102*(D14), 17,051–17,067. https://doi.org/10.1029/96jd03988
Kaufman, Y. J., Wald, A. E., Remer, L. A., Gao, B. C., Li, R. R., & Flynn, L. (1997). The MODIS 2.1-mu m channel - Correlation with visible reflectance for use in remote sensing of aerosol. *IEEE Transactions on Geoscience and Remote Sensing*, *35*(5), 1286–1298. https://doi.org/10.1109/36.628795
Kokhanovsky, A. A., Breon, F. M., Cacciari, A., Carboni, E., Diner, D., di Nicolantonio, W., et al. (2007). Aerosol remote sensing over land: A comparison of satellite retrievals using different algorithms and instruments. *Atmospheric Research*, *85*(3–4), 372–394. https://doi.org/10.1016/j.atmosres.2007.02.008
Konyukh, L. A., Yurevich, F. B., Cess, R. D., & Ardhan, H. (1979). Tropospheric aerosols - effects upon the surface and surface-atmosphere radiation budgets. *Journal of Quantitative Spectroscopy & Radiative Transfer*, *22*(5), 483–488. https://doi.org/10.1016/0022-4073(79)90085-2
Koren, I., Kaufman, Y. J., Remer, L. A., & Martins, J. V. (2004). Measurement of the effect of Amazon smoke on inhibition of cloud formation. *Science*, *303*(5662), 1342–1345. https://doi.org/10.1126/science.1089424
Kotchenova, S. Y., & Vermote, E. F. (2007). Validation of a vector version of the 6S radiative transfer code for atmospheric correction of satellite data. Part II. Homogeneous Lambertian and anisotropic surfaces. *Applied Optics*, *46*(20), 4455–4464. https://doi.org/10.1364/ao.46.004455
Kotchenova, S. Y., Vermote, E. F., Levy, R., & Lyapustin, A. (2008). Radiative transfer codes for atmospheric correction and aerosol retrieval: Intercomparison study. *Applied Optics*, *47*(13), 2215–2226. https://doi.org/10.1364/ao.47.002215
Kotchenova, S. Y., Vermote, E. F., Matarrese, R., & Klemm, F. J. Jr. (2006). Validation of a vector version of the 6S radiative transfer code for atmospheric correction of satellite data. Homogeneous Lambertian and anisotropic surfaces. *Applied Optics*, *45*(26), 6762–6774. https://doi.org/10.1364/ao.45.006762
Levy, R. C., Remer, L. A., Mattoo, S., Vermote, E. F., & Kaufman, Y. J. (2007). Second-generation operational algorithm: Retrieval of aerosol properties over land from inversion of moderate resolution imaging Spectroradiometer spectral reflectance. *Journal of Geophysical Research*, *112*, D13211. https://doi.org/10.1029/2006JD007811
Li, C. C., Lau, A. K. H., Mao, J. T., & Chu, D. A. (2005). Retrieval, validation, and application of the 1-km aerosol optical depth from MODIS measurements over Hong Kong. *IEEE Transactions on Geoscience and Remote Sensing*, *43*(11), 2650–2658. https://doi.org/10.1109/tgrs.2005.856627
Li, Z., Li, L., Zhang, F., Li, D., Xie, Y., & Xu, H. (2015). Comparison of aerosol properties over Beijing and Kanpur: Optical, physical properties and aerosol component composition retrieved from 12 years ground-based Sun-sky radiometer remote sensing data. *Journal of Geophysical Research: Atmospheres*, *120*, 1520–1535. https://doi.org/10.1002/2014JD022593
Li, Z., Zhao, X., Kahn, R., Mishchenko, M., Remer, L., Lee, K. H., et al. (2009). Uncertainties in satellite remote sensing of aerosols and impact on monitoring its long-term trend: A review and perspective. *Annales Geophysicae*, *27*(7), 2755–2770. https://doi.org/10.5194/angeo-27-2755-2009
Liepert, B. G., & Lohmann, U. (2001). A comparison of surface observations and ECHAM4-GCM experiments and its relevance to the indirect aerosol effect. *Journal of Climate*, *14*(6), 1078–1091. https://doi.org/10.1175/1520-0442(2001)014<1078:Acosoa>2.0.Co;2
Limbacher, J. A., & Kahn, R. A. (2017). Updated MISR dark water research aerosol retrieval algorithm part 1: Coupled 1.1km ocean surface chlorophyll a retrievals with empirical calibration corrections. *Atmospheric Measurement Techniques*, *10*(4), 1539–1555. https://doi.org/10.5194/amt-10-1539-2017
Liu, H., I. Laszlo, S. Kondragunta, L. A. Remer, and J. Huang (2012), Evaluation of Global VIIRS Aerosol EDR Product with MODIS and AERONET.
Lohmann, U., & Feichter, J. (2005). Global indirect aerosol effects: A review. *Atmospheric Chemistry and Physics*, *5*(3), 715–737. https://doi.org/10.5194/acp-5-715-2005
Mei, L., Xue, Y., Kokhanovsky, A. A., von Hoyningen-Huene, W., Istomina, L., de Leeuw, G., et al. (2013). Aerosol optical depth retrieval over snow using AATSR data. *International Journal of Remote Sensing*, *34*(14), 5030–5041. https://doi.org/10.1080/01431161.2013.786197
Melin, F., Zibordi, G., & Djavidnia, S. (2007). Development and validation of a technique for merging satellite derived aerosol optical depth from SeaWiFS and MODIS. *Remote Sensing of Environment*, *108*(4), 436–450. https://doi.org/10.1016/j.rse.2006.11.026
Morino, Y., Ueda, K., Takami, A., Nagashima, T., Tanabe, K., Sato, K., et al. (2017). Sensitivities of simulated source contributions and health impacts of PM2.5 to Aerosol Models. *Environmental Science & Technology*, *51*(24), 14,273–14,282. https://doi.org/10.1021/acs.est.7b04000
Nabat, P., Somot, S., Mallet, M., Sevault, F., Chiacchio, M., & Wild, M. (2015). Direct and semi-direct aerosol radiative effect on the Mediterranean climate variability using a coupled regional climate system model. *Climate Dynamics*, *44*(3–4), 1127–1155. https://doi.org/10.1007/s00382-014-2205-6
Noh, Y. M., Mueller, D., Shin, D. H., Lee, H., Jung, J. S., Lee, K. H., et al. (2009). Optical and microphysical properties of severe haze and smoke aerosol measured by integrated remote sensing techniques in Gwangju, Korea. *Atmospheric Environment*, *43*(4), 879–888. https://doi.org/10.1016/j.atmosenv.2008.10.058
Parsiani, H., & Mèndez, J. (2008). Aerosol size distribution using Lidar data and a typical Lidar assembly. *WSEAS Transactions on Systems*, *7*(11), 1218–1227.
Qin, K., M. Hu, L. Wu, L. Rao, H. Lang, L. Wang, B. Yang, and IEEE (2016), Satellite remote sensing of aerosol optical depth, SO_2 and NO_2 over China's Beijing-Tianjin-Hebei Region during 2002–2013, in *2016 IEEE International Geoscience and Remote Sensing Symposium*, edited, pp. 5727–5728, doi:https://doi.org/10.1109/igarss.2016.7730496.
Qiu, Y., Zhao, C., Guo, J., & Li, J. (2017). 8-year ground-based observational analysis about the seasonal variation of the aerosol-cloud droplet effective radius relationship at SGP site. *Atmospheric Environment*, *164*, 139–146. https://doi.org/10.1016/j.atmosenv.2017.06.002
Quaas, J., Boucher, O., Dufresne, J. L., & Le Trent, H. (2004). Impacts of greenhouse gases and aerosol direct and indirect effects on clouds and radiation in atmospheric GCM simulations of the 1930-1989 period. *Climate Dynamics*, *23*(7–8), 779–789. https://doi.org/10.1007/s00382-004-0475-0

Quinn, P. K., Coffman, D. J., Johnson, J. E., Upchurch, L. M., & Bates, T. S. (2017). Small fraction of marine cloud condensation nuclei made up of sea spray aerosol. *Nature Geoscience*, *10*(9), 674–679. https://doi.org/10.1038/ngeo3003

Randles, C. A., P. R. Colarco, A. D. Silva, A. M. Colarco, and R. C. Govindaraju (2009), Aerosol direct and semi-direct effects on climate in Asia in the NASA GEOS-5 model, paper presented at Agu Fall Meeting.

Rap, A., Scott, C. E., Spracklen, D. V., Bellouin, N., Forster, P. M., Carslaw, K. S., et al. (2013). Natural aerosol direct and indirect radiative effects. *Geophysical Research Letters*, *40*, 3297–3301. https://doi.org/10.1002/grl.50441

Rind, D., Balachandran, N. K., & Suozzo, R. J. (1992). Climate change and the middle atmosphere. Part II: The Impact of Volcanic Aerosols. *Journal of Climate*, *5*(3), 189–208. https://doi.org/10.1175/1520-0442(1992)005<0189:CCATMA>2.0.CO;2

Salma, I., Nemeth, Z., Weidinger, T., Kovacs, B., & Kristof, G. (2016). Measurement, growth types and shrinkage of newly formed aerosol particles at an urban research platform. *Atmospheric Chemistry and Physics*, *16*(12), 7837–7851. https://doi.org/10.5194/acp-16-7837-2016

Sayer, A. M., Hsu, N. C., Bettenhausen, C., Ahmad, Z., Holben, B. N., Smirnov, A., et al. (2012). SeaWiFS Ocean aerosol retrieval (SOAR): Algorithm, validation, and comparison with other data sets. *Journal of Geophysical Research*, *117*, D03206. https://doi.org/10.1029/2011JD016599

Schultze, M., & Rockel, B. (2018). Direct and semi-direct effects of aerosol climatologies on long-term climate simulations over Europe. *Climate Dynamics*, *50*(9–10), 3331–3354. https://doi.org/10.1007/s00382-017-3808-5

Shi, X., Zhao, C., Jiang, J. H., Wang, C., Yang, X., & Yung, Y. L. (2018). Spatial representativeness of PM2.5 Concentrations Obtained Using Observations From Network Stations. *Journal of Geophysical Research: Atmospheres*, *123*, 3145–3158. https://doi.org/10.1002/2017JD027913

Skupin, A., Ansmann, A., Engelmann, R., Seifert, P., & Mueller, T. (2016). Four-year long-path monitoring of ambient aerosol extinction at a central European urban site: Dependence on relative humidity. *Atmospheric Chemistry and Physics*, *16*(4), 1863–1876. https://doi.org/10.5194/acp-16-1863-2016

Spracklen, D. V., Carslaw, K. S., Poeschl, U., Rap, A., & Forster, P. M. (2011). Global cloud condensation nuclei influenced by carbonaceous combustion aerosol. *Atmospheric Chemistry and Physics*, *11*(17), 9067–9087. https://doi.org/10.5194/acp-11-9067-2011

Su, C., Su, L., Chen, L., Jia, S., Liu, C., & Yu, C. (2015). Retrieval of aerosol optical depth using NPP VIIRS data. *Journal of Remote Sensing*, *19*(6), 977–989.

Sun, L. (2006), Remote sensing of aerosols over urban areas, Institute of Remote Sensing and Digital Earth,Chinese Academy of Sciences.

Sun, L., Sun, C., Liu, Q., & Zhong, B. (2010). Aerosol optical depth retrieval by HJ-1/CCD supported by MODIS surface reflectance data. *Science China-Earth Sciences*, *53*(S1), 74–80. https://doi.org/10.1007/s11430-010-4134-5

Sun, L., Wei, J., Bilal, M., Tian, X., Jia, C., Guo, Y., & Mi, X. (2016). Aerosol optical depth retrieval over bright areas using Landsat 8 OLI images. *Remote Sensing*, *8*(1). https://doi.org/10.3390/rs8010023

Takemura, T., Nakajima, T., Dubovik, O., Holben, B. N., & Kinne, S. (2002). Single-scattering albedo and radiative forcing of various aerosol species with a global three-dimensional model. *Journal of Climate*, *15*(4), 333–352. https://doi.org/10.1175/1520-0442(2002)015<0333:Ssaarf>2.0.Co;2

Tanre, D., Deschamps, P. Y., Devaux, C., & Herman, M. (1988). Estimation of saharan aerosol optical-thickness from blurring effects in thematic mapper data. *Journal of Geophysical Research*, *93*(D12), 15,955–15,964. https://doi.org/10.1029/JD093iD12p15955

Tian, X., Sun, L., Liu, Q., & Li, X. (2018). Retrieval of high-resolution aerosol optical depth using Landsat 8 OLI data over Beijing. *Journal of Remote Sensing*, *22*(1), 51–63.

Tong, R. E. N., Ling, G. A. O., Chengcai, L. I., Jietai, M. A. O., Wanbiao, L. I., Guangming, S. H. I., et al. (2011). Retrieval of aerosol optical depth from Fengyun-2C geostationary satellite observation:Theory and implementation. *Acta Scientiarum Naturalium Universitatis Pekinensis*, *47*(4), 636–646.

Twomey, S. (1977). Influence of pollution on shortwave albedo of clouds. *Journal of the Atmospheric Sciences*, *34*(7), 1149–1152. https://doi.org/10.1175/1520-0469(1977)034<1149:Tiopot>2.0.Co;2

Veefkind, J. P., de Leeuw, G., Durkee, P. A., Russell, P. B., Hobbs, P. V., & Livingston, J. M. (1999). Aerosol optical depth retrieval using ATSR-2 and AVHRR data during TARFOX. *Journal of Geophysical Research*, *104*(D2), 2253–2260. https://doi.org/10.1029/98JD02816

Vermote, E. F., J. C. Roger, and J. P. Ray (2015), MODIS surface reflectance user's guide. version 1.4. http://modis-sr.ltdri.org/guide/MOD09_UserGuide_v1.4.pdf.

Vermote, E. F., and A. Vermeulen (1999), Atmospheric correction algorithm: Spectral reflectances (MOD09). Version 4.0. https://lpdaac.usgs.gov/sites/default/files/public/product_documentation/atbd_mod09.pdf.

Wang, F., Guo, J., Zhang, J., Huang, J., Min, M., Chen, T., et al. (2015). Multi-sensor quantification of aerosol-induced variability in warm clouds over eastern China. *Atmospheric Environment*, *113*, 1–9. https://doi.org/10.1016/j.atmosenv.2015.04.063

Wang, Q., Sun, L., Wei, J., Yang, Y., Li, R., Liu, Q., & Chen, L. (2017). Validation and accuracy analysis of global MODIS aerosol products over land. *Atmosphere*, *8*(12). https://doi.org/10.3390/atmos8080155

Wang, Y., Chen, L., Li, S., Wang, X., Yu, C., Si, Y., & Zhang, Z. (2017). Interference of heavy aerosol loading on the VIIRS aerosol optical depth (AOD) retrieval algorithm. *Remote Sensing*, *9*(4). https://doi.org/10.3390/rs9040397

Wang, Z., Li, Q., Wang, Q., Li, S., Chen, L., Zhou, C., et al. (2012). HJ-1 terrestrial aerosol data retrieval using deep blue algorithm. *Journal of Remote Sensing*, *16*(3), 596–610.

Wang, Z., Liangfu, C., Ying, Z., Dong, H. A. N., & Xingfa, G. U. (2008). Urban surface aerosol monitoring using DDV method from MODIS data. *Remote Sensing Technology and Application*, *23*(3), 284–288.

Wei, J., Huang, B., Sun, L., Zhang, Z., Wang, L., & Bilal, M. (2017). A simple and universal aerosol retrieval algorithm for Landsat series images over complex surfaces. *Journal of Geophysical Research: Atmospheres*, *122*, 13,338–13,355. https://doi.org/10.1002/2017jd026922

Wei, J., & Sun, L. (2017). Comparison and evaluation of different MODIS aerosol optical depth products over the Beijing-Tianjin-Hebei region in China. *IEEE Journal of Selected Topics in Applied Earth Observations and Remote Sensing*, *10*(3), 835–844. https://doi.org/10.1109/jstars.2016.2595624

Wei, J., Sun, L., Huang, B., Bilal, M., Zhang, Z., & Wang, L. (2018). Verification, improvement and application of aerosol optical depths in China part I: Inter-comparison of NPP-VIIRS and aqua-MODIS. *Atmospheric Environment*, *175*, 221–233. https://doi.org/10.1016/j.atmosenv.2017.11.048

Xue, H., Feingold, G., & Stevens, B. (2008). Aerosol effects on clouds, precipitation, and the organization of shallow cumulus convection. *Journal of the Atmospheric Sciences*, *65*(2), 392–406. https://doi.org/10.1175/2007jas2428.1

Xue, Y., Guo, J., & Zhang, X. (2009). Aerosol optical thickness retrieval over non-Lambertian land surface with synergistic use of AATSR radiance measurements and MODIS derived albedo model parameters. *Atmospheric Research*, *93*(4), 736–746. https://doi.org/10.1016/j.atmosres.2009.02.013

Yan, W., Yang, L., Chen, J., Wang, X., Wen, L., Zhao, T., & Wang, W. (2017). Aerosol optical properties at urban and coastal sites in Shandong Province, Northern China. *Atmospheric Research*, *188*, 39–47. https://doi.org/10.1016/j.atmosres.2016.12.011

Yang, X., Zhao, C., Zhou, L., Li, Z., Cribb, M., & Yang, S. (2018). Wintertime cooling and a potential connection with transported aerosols in Hong Kong during recent decades. *Atmospheric Research*, *211*, 52–61. https://doi.org/10.1016/j.atmosres.2018.04.029

Yang, X., Zhao, C., Zhou, L., Wang, Y., & Liu, X. (2016). Distinct impact of different types of aerosols on surface solar radiation in China. *Journal of Geophysical Research: Atmospheres*, *121*, 6459–6471. https://doi.org/10.1002/2016JD024938

Yang, Y., Sun, L., Zhu, J., Wei, J., Su, Q., Sun, W., et al. (2017). A simplified Suomi NPP VIIRS dust detection algorithm. *Journal of Atmospheric and Solar-Terrestrial Physics*, *164*, 314–323. https://doi.org/10.1016/j.jastp.2017.08.010

Yang, Y., Zhao, C., Dong, X., Fan, G., Zhou, Y., Wang, Y., et al. (2019). Toward understanding the process-level impacts of aerosols on microphysical properties of shallow cumulus cloud using aircraft observations. *Atmospheric Research*, *221*, 27–33. https://doi.org/10.1016/j.atmosres.2019.01.027

Yu, X., Lu, R., Liu, C., Yuan, L., Shao, Y., Zhu, B., & Lei, L. (2017). Seasonal variation of columnar aerosol optical properties and radiative forcing over Beijing, China. *Atmospheric Environment*, *166*, 340–350. https://doi.org/10.1016/j.atmosenv.2017.07.011

Zhang, H., Kondragunta, S., Laszlo, I., Liu, H., Remer, L. A., Huang, J., et al. (2016). An enhanced VIIRS aerosol optical thickness (AOT) retrieval algorithm over land using a global surface reflectance ratio database. *Journal of Geophysical Research: Atmospheres*, *121*, 10,717–10,738. https://doi.org/10.1002/2016JD024859

Zhang, H., Wang, Z., Zhang, F., & Jing, X. (2015). Impact of four-stream radiative transfer algorithm on aerosol direct radiative effect and forcing. *International Journal of Climatology*, *35*(14), 4318–4328. https://doi.org/10.1002/joc.4289

Zhao, C., & Garrett, T. J. (2015). Effects of Arctic haze on surface cloud radiative forcing. *Geophysical Research Letters*, *42*, 557–564. https://doi.org/10.1002/2014GL062015

Zhao, C., Klein, S. A., Xie, S., Liu, X., Boyle, J. S., & Zhang, Y. (2012). Aerosol first indirect effects on non-precipitating low-level liquid cloud properties as simulated by CAM5 at ARM sites. *Geophysical Research Letters*, *39*, L08806. https://doi.org/10.1029/2012GL051213

Zhao, C., Qiu, Y., Dong, X., Wang, Z., Peng, Y., Li, B., et al. (2018). Negative aerosol-cloud r(e) relationship from aircraft observations over Hebei, China. *Earth and Space Science*, *5*(1), 19–29. https://doi.org/10.1002/2017ea000346

Zhao, C., Zhao, L., & Dong, X. (2019). A case study of stratus cloud properties using in situ aircraft observations over Huanghua, China. *Atmosphere*, *10*(1), 19. https://doi.org/10.3390/atmos10010019

Zheng, C., Zhao, C., Zhu, Y., Wang, Y., Shi, X., Wu, X., et al. (2017). Analysis of influential factors for the relationship between PM2.5 and AOD in Beijing. *Atmospheric Chemistry and Physics*, *17*(21), 13,473–13,489. https://doi.org/10.5194/acp-17-13473-2017